IEEE Access
Multidisciplinary ⋮ Rapid Review ⋮ Open Access Journal

Received 27 April 2025, accepted 13 June 2025, date of publication 16 June 2025, date of current version 23 June 2025.

Digital Object Identifier 10.1109/ACCESS.2025.3580352

RESEARCH ARTICLE

Design of a Controllable Axial-Flux Halbach Array for Magnetic Suspension Tasks

WILL FLANAGAN[1], (Member, IEEE), HE KAI LIM[1], CAMERON R. TAYLOR[2], AND TYLER R. CLITES[1,3]

[1]Department of Mechanical and Aerospace Engineering, University of California at Los Angeles, Los Angeles, CA 90095, USA
[2]Joint Department of Biomedical Engineering, University of North Carolina at Chapel Hill and North Carolina State University, Chapel Hill, NC 27599, USA
[3]Department of Orthopaedic Surgery, University of California at Los Angeles, Los Angeles, CA 90095, USA

Corresponding author: Will Flanagan (wflan@ucla.edu)

This work was supported in part by the National Science Foundation Graduate Research Fellowship Program under Grant DGE-2034835, in part by U.S. Department of Defense under Grant W81XWH2220046, and in part by the National Science Foundation Disability and Rehabilitation Engineering Program under Grant 2144015.

ABSTRACT Magnetic fields enable force application without mechanical connection. By this means, electromagnets apply force across a distance, but require continuous power to maintain constant force. In contrast, switchable permanent magnet mechanisms allow unpowered constant force application, but are typically used in close-range (small gap) applications. Hence, a device enabling low-power force application over greater distances (large gap) is needed. To meet this need, we introduce an adjustable magnetic actuator called a controllable, axial-flux Halbach array (CAHA). The novelty of our design lies in the concentric nesting of two axial-flux Halbach rings. By nesting these rings, the magnetic field extends out axially on one side, with a strength dependent on the relative rotation between the rings. To demonstrate how this mechanism performs in magnetic suspension tasks, we simulated a CAHA design model, compared this design model to alternative magnetic actuators, swept geometric parameters of the design, and empirically characterized a CAHA prototype. Our simulations show that our device required much less power than an electromagnet for low-frequency ($<$16 Hz) tasks, with an up to 93% reduction in average power for a 5 Hz task. The CAHA model also had force densities up to 2.3x higher than a switchable magnet for large-gap ($\geq$10 mm) applications. In empirical tests of the CAHA, magnetic performance closely matched our simulations. These results represent an introduction to the CAHA design that could improve magnetic suspension systems for low-frequency, large-gap applications.

INDEX TERMS Adjustable permanent magnet array, Halbach array, large-gap magnetic suspension.

I. INTRODUCTION

Active suspension of magnetic materials across large gaps ($\geq$10 mm) is an important but challenging problem due to magnetic fields deteriorating quickly and nonlinearly as a function of distance. These situations are encountered in many applications, such as robotic manipulation [1], structure-climbing robots [2], [3], non-contact material handling [4], MagLev trains [5], and when ferromagnetic materials are embedded within non-magnetic material [6]. A major problem in these applications is producing strong fields in a manner that is both controllable and power-efficient. Most systems utilize electromagnets as the magnetic field source because they have no moving parts and are easy to modulate by adjusting the applied current. Electromagnets are not ideal for sustained force applications, however, since maintaining high fields requires high electrical power [7].

To address the need for low-power, strong, and variable magnetic field sources, we introduce the controllable axial-flux Halbach array (CAHA): a novel adjustable permanent magnet mechanism for magnetic suspension. Our CAHA design consists of two nested axial-flux Halbach rings. Together, these produce the characteristic one-sided field of Halbach arrays [8], [9] that extends out axially above

The associate editor coordinating the review of this manuscript and approving it for publication was Valentine Novosad.

the array. While single axial-flux Halbach rings have been used in permanent magnet machines [10], [11], our nested axial-flux Halbach rings allow for adjustment of the resultant field by rotating the rings relative to one another. This operating principle is the same as "magic cylinders" used in particle accelerators [8], [12] and magnetic refrigeration devices [13], [14]. These magic cylinders are composed of two nested Halbach rings, each with radial/tangential Halbach patterns (not axial-flux). Each ring in isolation creates a strong multipole field within its inner bore [15] while minimizing the field outside. By nesting one ring inside the other, the axial rotation of one ring relative to the other varies the constructive or destructive interference between each ring's field within the bore. This results in the strength and direction of the field within the bore to be a function of this ring angle. In contrast to magic cylinders, the use of axial-flux Halbach rings (CAHA) rather than a radial/tangential pattern (magic cylinder) positions the controllable field axially outside the rings, making the CAHA more useful for interacting with the external environment.

Adjustable permanent magnet mechanisms, such as a CAHA or magic cylinder, are generally less power-intensive than electromagnets because the magnetic field depends on the relative position of magnetic elements rather than an electrical current [7]. This means that power for adjustable permanent magnets is only required to *change* the field, and that *maintaining* a constant field require no power at all. It must be noted, however, that interaction forces and torques between the permanent magnet elements do exist and must be actively counteracted during use [16], although the use of clutches, friction, or non-backdrivable transmissions can passively counteract these forces when the magnets are stationary. Due to their low power operation, adjustable permanent magnet –but non-Halbach– alternatives to electromagnets exist for industrial material handling in the form of switchable magnets (SMs) like the MagSwitch® [17] and flux-path control devices [18]. One common SM design is composed of two diametrically-magnetized cylinders that are stacked vertically and surrounded by a ferromagnetic yoke. The yoke redirects the flux axially to the top of the cylinders, and is designed such that the field above the cylinders varies from a minimum to a maximum when one cylinder is rotated 180°. This specific design has been used for robotics applications like climbing robots [2], [3] or in pick-and-place robotic arms [1], [19].

When compared to SMs and flux-path control devices, adjustable magnets using Halbach arrays may have several advantages for magnetic suspension tasks. First, the self-shielding, one-sided flux of Halbach arrays allows the field to be concentrated in the region of interest without the need for ferromagnetic yokes (SMs) or moveable leaves (flux-path control). Eliminating yokes and leaves maximizes the amount of permanent magnetic material in the device, which can decrease mass and increase force densities. Halbach arrays could also outperform SMs at generating high forces across air gaps, because Halbach arrays have been used to produce fields that extend farther into space compared to other array patterns [20], while SMs are generally used in direct contact with ferromagnets [1]. Large-gap force transmission is important for magnetic suspension because the ferromagnetic material of interest could be behind a non-ferromagnetic material (e.g. paint, protective covers) [6]. Within previously described adjustable magnets that utilize a Halbach pattern, a *planar* Halbach array using many magnetized rods has been described in literature [21], however that planar design contains many moving parts, complicating its translation to a physical device compared to our proposed CAHA.

In this paper, we introduce a generalized design of our novel CAHA device. The primary significance of this work is the CAHA design itself. To investigate the potential applications of our device, we first use simulation software to compare the performance of our mechanism to that of an electromagnet and to a switchable magnet in various magnetic suspension tasks. Then, with an understanding of the operating regimes suited for our device, we explore how design parameters could affect magnetic suspension performance. Finally, we build and test a CAHA prototype, verifying that the simulated behavior of the mechanism translates to a physical device.

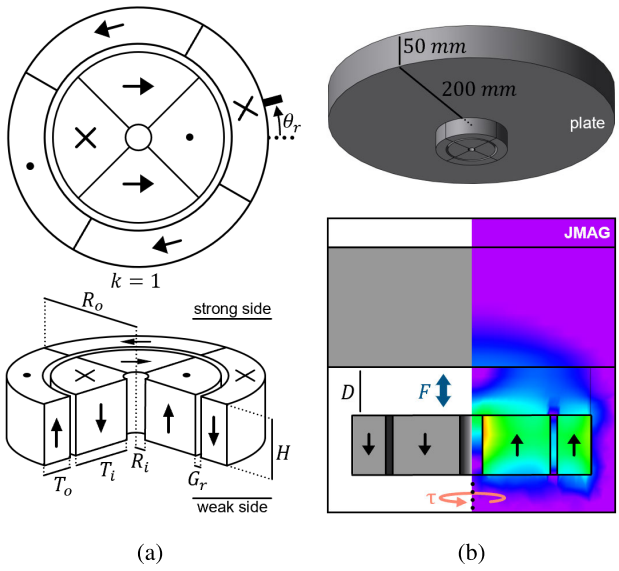

FIGURE 1. A controllable, axial-flux Halbach array (CAHA). (a) Generic $k = 1$ CAHA and its design parameters shown in the anti-aligned configuration. (b) The simulated magnetic suspension task placed a ferromagnetic cylindrical plate above the array. The section view (bottom) shows the gap distance D, attraction force F exerted on the plate, and the ring turning torque τ along with a typical magnetic flux density contour plot produced when the rings are aligned. Black arrows denote magnetization.

II. METHODS

A. SYSTEM OVERVIEW

Our CAHA device is composed of two nested axial-flux Halbach rings (Fig. 1a) that in isolation form a strong field

above the array and a weak field below it. The device configuration is defined by the rotation angle between the two rings (θ_r), where $\theta_r = 0°$ is defined as the rings being anti-aligned. Relevant design parameters of the CAHA are the outer radius (R_o), ring thickness ratio (T_o/T_i), ring height (H), gap between the rings (G_r), and inner bore radius (R_i). The Halbach pattern used for each ring consists of segments with magnetization 90 degrees apart, and the wavenumber (k) defines the number of times this pattern repeats for each ring. We chose NdFeB grade N52M [22] for each segment and verified that no local demagnetization occurred using criteria from Bjørk et al. [23]. This demagnetization analysis is presented in Supplementary Fig. S1.

To evaluate this device, we modeled a general magnetic suspension task (Fig. 1b) involving the CAHA positioned below a ferromagnetic (400 series stainless steel [SS400]) cylindrical plate. The gap distance between the bottom of the plate and top of the array is D and the plate has a 200 mm radius and 50 mm height. We chose these dimensions such that the plate was pseudo-infinite relative to the CAHA. All tasks were simulated using static 3D magnetic field analyses in the software JMAG (JSOL Corporation, Tokyo, Japan). In each simulation, the axial force exerted on the plate (F) and the torque required to turn a ring (τ) were calculated using nodal forces and nodal torques, respectively. We evaluated performance primarily by the maximum force (F_{max}), the range of forces ($F_{max} - F_{min}$) produced over the range of ring angles θ_r, and the turning torque (τ).

TABLE 1. Baseline parameters for the CAHA design model and manipulation task.

k	H	R_i	G_r	R_o	T_o/T_i	D
1	25 mm	5 mm	3 mm	50 mm	0.5625	20 mm

The baseline parameter values for our simulated CAHA are listed in Table 1. We set the overall size (R_o and H) based on a desired device envelope of 50 mm outer radius and 25 mm height. While this envelope is arbitrary due to the scope of this paper being to introduce the general design, it represents a potential design constraint on the size of the magnetic source. The wavenumber was set to $k = 1$ to model the simplest array design (each ring has one cycle of the Halbach pattern). We determined the thickness ratio (T_o/T_i) by sampling various values while keeping all other parameters constant and choosing the value with the highest force range (Supplementary Fig. S2). The ring gap (G_r) was set to 3 mm based on previous literature to balance the higher magnetic interference, constructive or destructive, between the inner and outer rings that occurs with smaller ring gaps at the expense of higher turning torques [14]. The inner bore radius (R_i) was set to 5 mm to allow for a driveshaft in potential CAHA-based actuator designs. These design parameters resulted in a combined mass of 1.34 kg for the two CAHA rings. The nominal gap distance of 20 mm provides a large gap compared to the dimensions of our array. It must be noted that this device is only an example from which we introduce and investigate the properties of the CAHA, with no claims of optimality.

To understand the general operation of this $k = 1$ baseline array, we simulated the magnetic suspension task over the range of ring angles from anti-aligned ($\theta_r = 0°$) to aligned ($\theta_r = 180°$). At each θ_r, we reported axial plate force and turning torque.

B. ELECTROMAGNET COMPARISON

Our first investigation for the baseline CAHA compared its performance to that of an electromagnet. Because the operating principles between the two devices are different —an electromagnet can produce infinite force given infinite power and the CAHA only requires power to change the field— we explored the power considerations of each device as a function of the frequency of the suspension task. Specifically, we simulated a sinusoidal load task covering the full force range of the CAHA at a 20 mm gap, and varied the frequency (0-20 Hz) to determine the frequencies where one device required lower average power than the other.

For the electromagnet, a generic design, consisting of a ferromagnetic core (SS400), copper coil, and shell (SS400), was modeled in JMAG. The outer envelope of the electromagnet was the same as our baseline CAHA ($R_o = 50$ mm, $H = 25$ mm). To avoid comparing the CAHA to a poor electromagnet design, we sampled each parameter in a multi-dimensional sweep and selected the five combinations of parameters that produced the highest force at 500 W power for a 20 mm gap distance. The chosen electromagnet designs had greater mass than the baseline CAHA (1.34 kg for the CAHA and 1.56 kg for the electromagnets). We then characterized the force vs. power relationship of each of the five designs by calculating the axial plate force resulting from powers between 0 W and 6 kW in JMAG simulations. Detailed information on the electromagnet simulation process can be found in Supplementary Materials. Given a desired loading profile of axial plate force over time, the power at each point in time was found by interpolating that force vs. power relationship. This reduced the electromagnet to a 0^{th} order system, but this was an appropriate simplification given the low inductance of the electromagnetic coil and the relatively low frequencies used.

To determine the power requirements of our CAHA mechanism for a loading cycle, we modeled a CAHA-based actuator in which a brushless DC motor directly rotates one of the rings. The chosen motor was the U8-KV100 (T-motor, Nanchang, Jiangxi, China) since this motor is a suitable size (43.5 mm radius, 26 mm height), lightweight (240 g), and has a published characterization [24] such that we could create an accurate motor model. Adding the motor to the CAHA rings brought the mass of the CAHA-based actuator (1.58 kg) close to that of the electromagnets (1.56 kg). To calculate the power dissipated (Q) for a given rotor load torque (T_l) and

rotor angle profile over time (θ_m), the motor model considers the motor's electromechanical parameters,

$$T_m = T_l/\eta + J_m\ddot{\theta}_m + b\dot{\theta}_m \rightarrow i = T_m/k_t \rightarrow Q = i^2\,R, \quad (1)$$

where T_m is the motor torque, η is a conservative estimate of actuator efficiency ($\eta = 0.9$), J_m is the rotor inertia ($J_m = 1.2\times10^{-4}\ kg\cdot m^2$), b is the rotor damping ($b = 0.16\ mNm/(rad/s)$), i is the motor current, k_t is the torque constant ($k_t = 0.14\ Nm/A$), and R is the terminal resistance of the motor ($R = 0.186\ \Omega$). Because the system is direct drive, $\theta_m = \theta_r$. The rotor load torque is composed of two terms: the turning torque of the CAHA ring (T_r), which is a function of ring angle, and the torque required to accelerate the inertia of the rings:

$$T_l = T_r(\theta_r) + J_{ring}\ddot{\theta}_r. \quad (2)$$

We used JMAG simulations to determine both the axial plate force and the ring turning torque as a function of ring angle, with the gap distance set to 20 mm. We then used this information to convert our desired axial plate force loading profiles into ring angle profiles. To calculate the ring inertia torque, we numerically differentiated these ring angle profiles twice to compute the angular acceleration of the rings. The rotational inertia (J_{ring}) of our proposed device varies based on the specific implementation: either the outer ring rotates with the inner ring fixed ($J_o = 1.3\times10^{-3}\ kg\cdot m^2$), or the inner ring rotates with the outer ring fixed ($J_i = 3.5\times10^{-4}\ kg\cdot m^2$). We tested both cases to capture the boundaries of operation for the CAHA.

C. SWITCHABLE MAGNET COMPARISON

Our second investigation for the baseline CAHA was comparing device performance to that of a switchable magnet (SM), because these devices are commonly used in material handling and have also been incorporated into robotic manipulators [1], [19]. A generic SM design [17] was modeled in JMAG and parameterized. Since this SM operates on a similar principle to our proposed array, with the produced field being a function of the angle between two diametrically magnetized discs, we directly compared the performance of the two architectures within different gap distance regimes. The disc magnets were set to N52M-grade NdFeB to match the CAHA segments and the ferromagnetic shell was set to S15C (AISI 1015) carbon steel. To choose SM designs for comparison, we selected the five designs with the highest force range ($F_{max} - F_{min}$) at a 20 mm gap distance from a multi-dimensional sweep. The modeled SMs were equal in size to the baseline CAHA ($R_o = 50$ mm, $H = 25$ mm) and were similar in mass to the baseline CAHA (1.34 kg for the CAHA and 1.35-1.37 kg for the SMs). More information on the SM simulation can be found in Supplementary Materials. For the suspension task detailed previously, we performed simulations at various magnet angles and recorded the axial plate force and turning torque of the SM. We then ran simulations and recorded the maximum and minimum axial plate forces of the devices for gap distances varying from 1-50 mm.

TABLE 2. Parameters for the CAHA prototype.

k	H	R_i	G_r	R_o	T_o/T_i	NdFeB
1	15 mm	5 mm	3.5 mm	35 mm	0.963	N52M

D. CAHA DESIGN ANALYSIS

1) WAVENUMBER

Using the baseline CAHA, we also explored the effects of changing the wavenumber (k) of each ring. The wavenumber, defined as the number of cycles per ring of the Halbach pattern, was set to either one (baseline), two, or three with all other parameters kept constant. First, we swept ring angle for each array at a 20 mm gap distance to compare the axial plate force and turning torque profiles. Next, we tested how gap distance affected the force range and the maximum ring torque for each of the three arrays by sweeping gap distances from 1 to 50 mm. At each gap distance, we simulated the magnetic field for ring angles corresponding to the maximum force, minimum force, and maximum torque conditions.

2) PARAMETER SWEEP

To understand how each of the geometric design parameters contribute to performance, we conducted a one-dimensional parameter sweep about the baseline design. For each parameter, we evaluated performance as the parameter of interest was varied within a design range. All other parameters were kept constant. Performance was evaluated by the maximum force, force range, maximum turning torque, and device mass.

E. PHYSICAL TESTING

Using the insight gained in the previous sections, we designed and fabricated a $k = 1$ CAHA for a magnetic suspension task. Within the scope of this paper, this prototype CAHA serves as a model to verify our simulation procedure; its specific application will be published in future work. Table 2 shows the parameters of the prototype. To confirm that the magnetic behaviors seen in simulations translated to the physical device, we characterized the array by measuring the axial force exerted on a large plate and the torque required to turn the CAHA inner ring over its 180° ring angle range. These curves were measured for gap distances of 5, 10, 15, and 20 mm, then compared to simulation results for the corresponding CAHA and plate geometries. In our testing setup, the CAHA was mounted to a table, and a grade 420 ferromagnetic stainless steel plate with 280 mm diameter and 50 mm height was placed above the array as in Fig. 1b. We mounted the plate to the end of a robotic manipulator (KR210, KUKA Robotics Corp.) such that we could control the gap distance between the top of the CAHA and the bottom of the plate. The inner ring of the CAHA prototype was turned quasi-statically at $1°/s$ by a motor through a 10:1

planetary gear reducer. The turning torque and ring angle of the CAHA was measured by an in-line torque sensor and the motor encoder, respectively. A load cell on the manipulator end effector measured the axial force on the ferromagnetic plate.

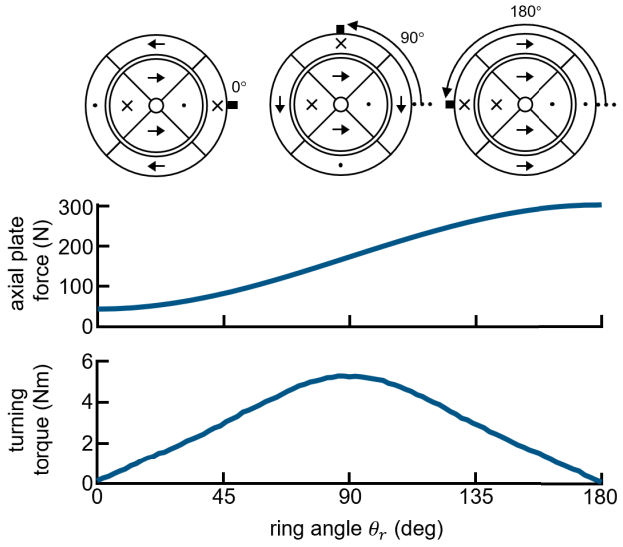

FIGURE 2. Operating principle of a CAHA with a wavenumber of $k = 1$ at a 20 mm gap distance. As the rings rotate from anti-aligned ($\theta_r = 0°$) to aligned ($\theta_r = 180°$), the axial plate force increases from a minimum to a maximum. The turning torque for this device is also a function of θ_r.

III. RESULTS

A. SYSTEM OVERVIEW

As shown in Fig. 2, our baseline CAHA produced a simulated minimum force of 44 N at a 20 mm gap when the rings were anti-aligned ($\theta_r = 0°$). Attractive force increased to a maximum of 303 N when the rings were aligned ($\theta_r = 180°$). The two rings had a combined mass of 1.34 kg. The turning torque was positive and varied with θ_r, reaching a maximum torque of 5.3 Nm near $\theta_r = 90°$. The positive turning torque from $\theta_r = 0°$ to 180° means that $\theta_r = 0°$ is a stable equilibrium, while $\theta_r = 180°$ is an unstable equilibrium.

B. ELECTROMAGNET COMPARISON

To produce the 2 Hz sinusoidal force profile shown as an example in Fig. 3a, electromagnets required peak powers near 5 kW while the CAHA configurations required around 400 W peak. Interestingly, the power profile for the CAHA configurations has a frequency double that of the force profile because the turning torque is out of phase with the force, as viewed with respect to the ring angle (see Fig. 2). Additional sharp peaks also appear at the points where the ring changes velocity. At frequencies less than 9 Hz for the outer ring configuration and 16 Hz for the inner ring configuration, the CAHA required much less average power than the electromagnets (Fig. 3b). For a 5 Hz loading profile, the outer ring CAHA required 83% less power than the

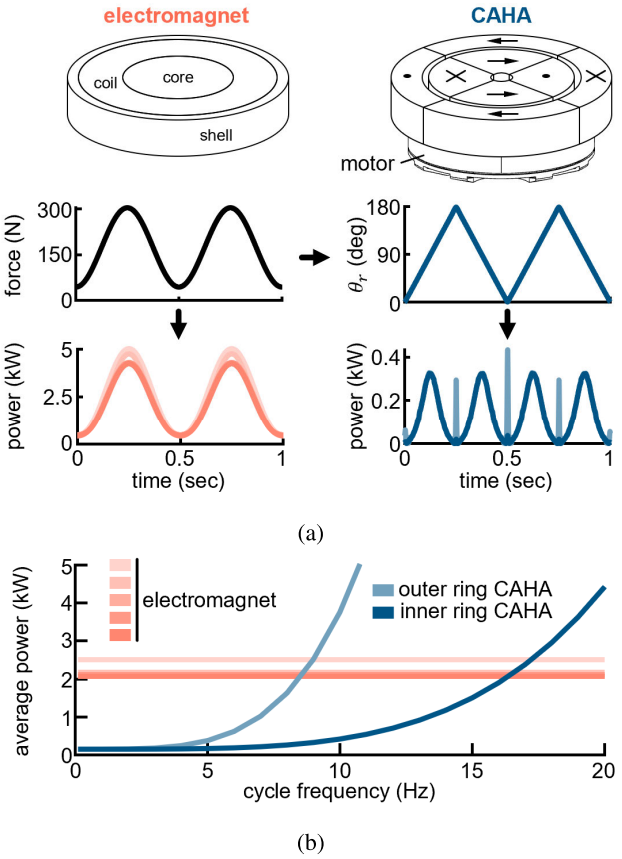

FIGURE 3. Power requirements of a CAHA-based actuator vs. electromagnets of comparable size. (a) An example 2 Hz sinusoidal force profile, top left, was converted to a power profile for the electromagnets, bottom left, using each design's force vs. power relationship. For the CAHA, the force profile was converted to a ring angle profile, top right, using its force vs. angle relationship. This angle over time profile was used to drive a motor model to calculate the power profile, bottom right. (b) Average power as a function of cycle frequency for electromagnets and the two CAHA configurations: rotating either the outer ring or the inner ring.

best electromagnet (0.36 kW compared to 2.04 kW). The inner ring CAHA produced this profile with 93% less power (0.15 kW compared to 2.04 kW).

C. SWITCHABLE MAGNET COMPARISON

Compared to the baseline CAHA at a 20 mm gap distance, the SM designs produced lower maximum forces and required higher turning torques (Fig. 4a). In the minimum force configuration, however, the SM designs all achieved near-zero forces. At gap distances below 5 mm, SM designs had force ranges in excess of 1000 N (Fig. 4b). These were much greater than the baseline CAHA array, where the force range diminishes at low gaps and may be negative (defined as the force at $\theta_r = 0°$ being larger than the force at $\theta_r = 180°$). For gap distances larger than 5 mm, the baseline CAHA had higher maximum forces and higher force ranges than the SM designs. At a gap distance of 10 mm, the CAHA produced a maximum force of 836 N while the SM designs had a maximum force of 363 N. Regarding force density at this gap

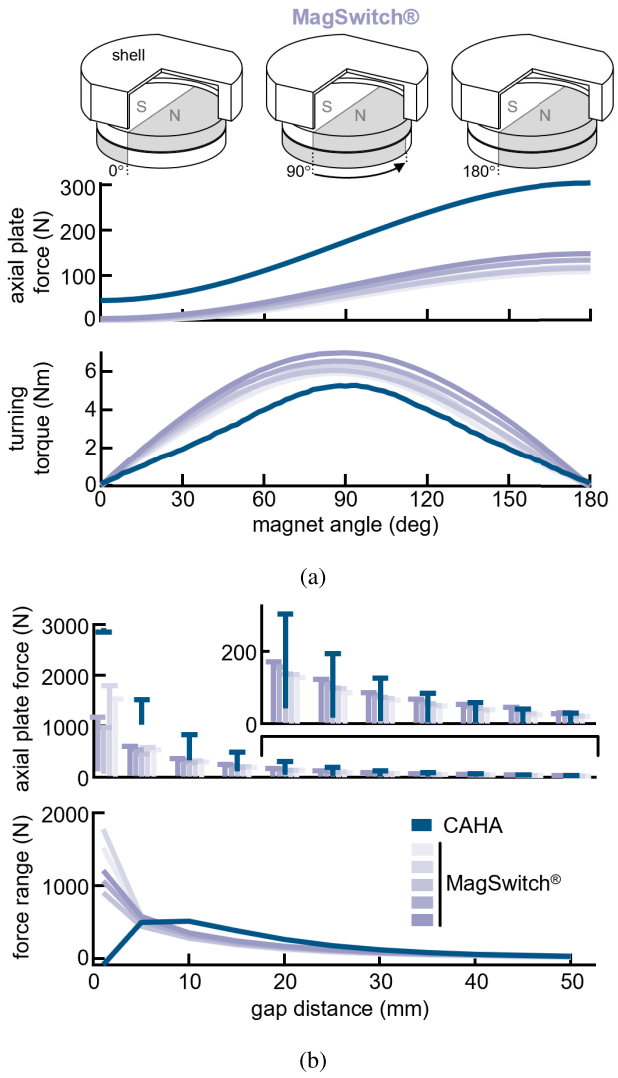

FIGURE 4. Switchable magnet (SM) comparison. (a) Exploded view diagrams of an example SM design (above) at different magnet angles demonstrate its operating principle. The plots below the diagrams show the SM axial plate forces and torques at a 20 mm gap distance as a function of magnet angle. The CAHA curves from Fig. 2 are superimposed. (b) Axial plate force and force range vs. gap distance. In the axial force plot, the horizontal bar denotes a magnet or ring angle of 180° (usually the maximum force) while the vertical bar length denotes the force range as this angle goes to 0°. The inset shows axial plate force for 20 to 50 mm gaps. Force range is the force when the magnets are aligned (180°) minus the force when the magnets are anti-aligned (0°).

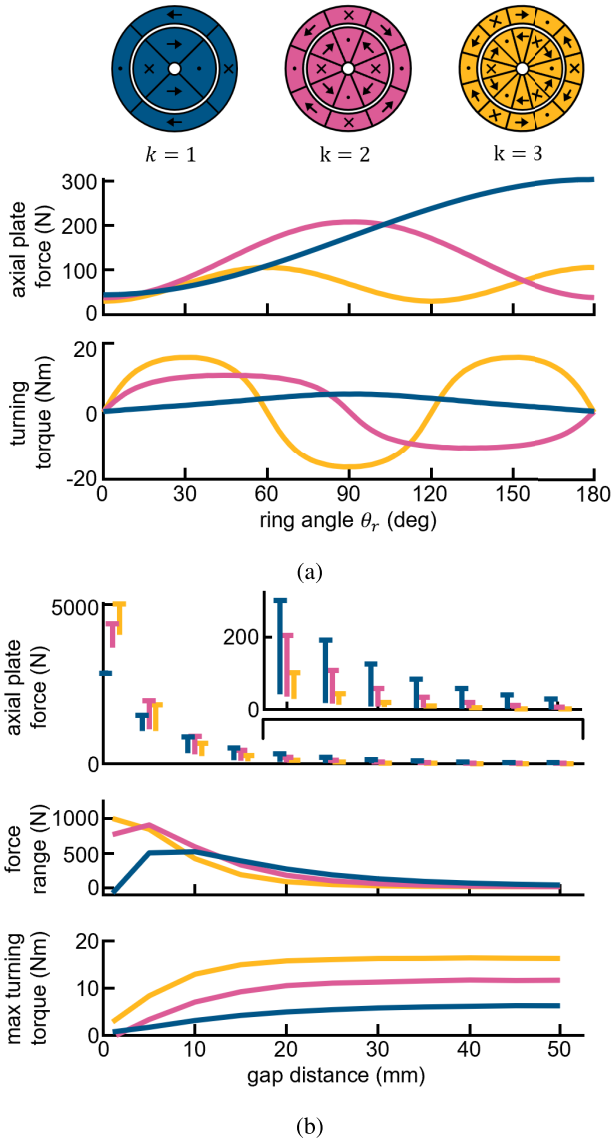

FIGURE 5. Effect of the wavenumber (k) on CAHA performance. (a) Axial plate force and turning torque as a function of ring angle at a distance of 20 mm. Rings are anti-aligned at $\theta_r = 0$ and aligned after rotations of $180°/k$. (b) Axial plate force, force range, and maximum turning torque vs. gap distance. In the axial force plot, the horizontal bar denotes a ring angle of $180°/k$ (usually the maximum force) while the vertical bar length denotes the force range as ring angle goes to 0°. The inset shows axial plate force for 20-50 mm gaps. Force range is the force when the rings are aligned ($180°/k$) minus the force when the rings are anti-aligned (0°). Maximum turning torque is the torque when the rings are half-aligned ($90°/k$).

distance, the CAHA had 2.3x the force density of the most force-dense SM (624 N/kg for CAHA vs. 266 N/kg for SM).

D. CAHA DESIGN ANALYSIS

1) WAVENUMBER

The $k = 1$ CAHA produced higher forces and force ranges than the $k = 2$ and $k = 3$ designs for gaps of 15 mm or larger (see Fig. 5a) and required less turning torque regardless of gap distance (see Fig. 5b). For low gap distances, arrays with higher k produced both higher forces and higher force ranges (Fig. 5b). As seen in Fig. 5a, increasing the wavenumber reduces the angular displacement between the minimum and maximum force configurations as $180°/k$.

2) PARAMETER SWEEP

One-dimensional sweeps of each geometric parameter (Fig. 6), found that all four performance metrics (maximum force, force range, maximum turning torque, and mass) followed the same trends within each parameter. As the magnet height and outer radius increased, all metrics increased.

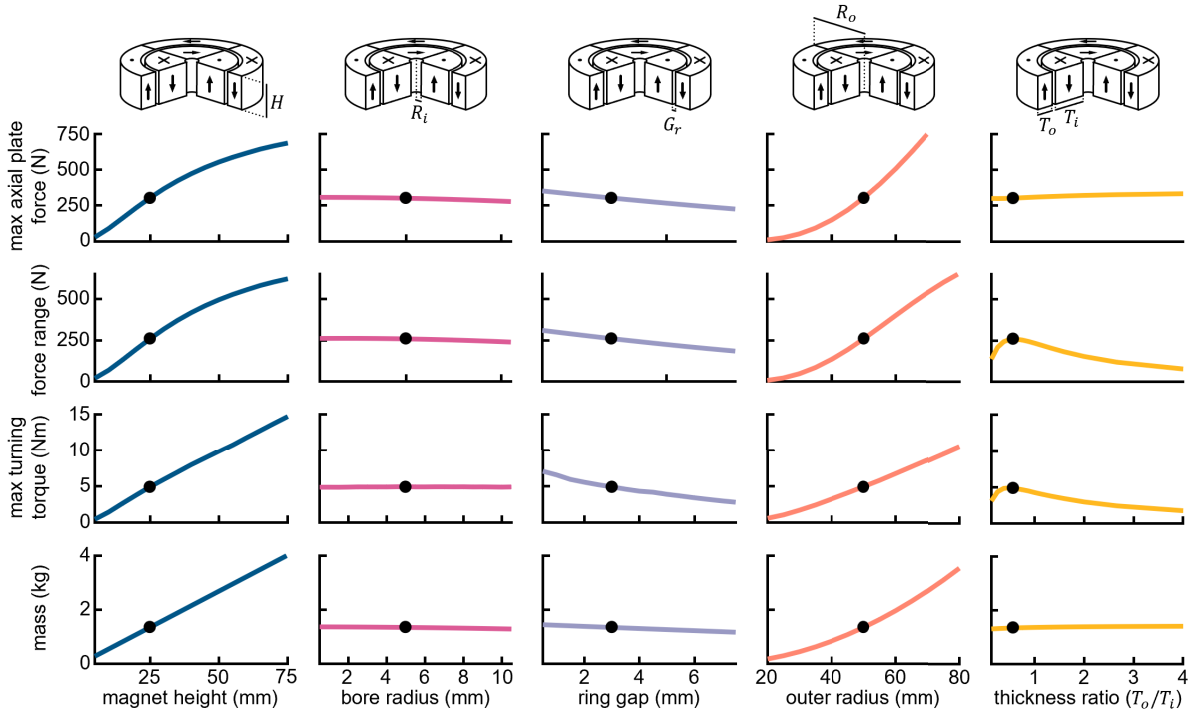

FIGURE 6. 1-dimensional sweeps for each geometric parameter about the $k = 1$ baseline design at a gap distance of 20 mm. The maximum axial plate force is the force produced when the rings are aligned ($\theta_r = 180°$). The force range is the maximum axial plate force minus the force produced when the rings are anti-aligned ($\theta_r = 0°$). The maximum turning torque is the torque required to turn the rings at $\theta_r = 90°$, which corresponded to the maximum torque in simulation results. The mass is the combined mass of the two rings. Each parameter was independently varied while the other parameters were kept constant. The dot on each plot denotes the baseline value.

Increasing either bore radius or ring gap reduced each metric, with ring gap having a greater effect. The thickness ratio between the outer and inner rings was maximized the force range and the turning torque near $T_o/T_i = 0.5625$.

E. PHYSICAL TESTING

Characterization of the CAHA prototype showed close agreement between the physical device and JMAG simulation predictions, in both axial plate force and ring turning torque as a function of ring angle (Fig. 7). This agreement held for all tested gap distances, such that the average RMSE between the measured and simulated data over the four gap distances was 9.64 N for forces and 0.05 Nm for torques. Magnetic viewing film placed at 27.5 mm above the array in the absence of the plate clearly shows the increase in magnetic flux density as the inner ring is rotated. Images of the magnetic viewing film for other heights above the CAHA are shown in Supplementary Fig. S5.

IV. DISCUSSION

In this paper, we introduce and explore a novel mechanism called the controllable, axial-flux Halbach array (CAHA). We created this mechanism to address the need for low-power, high-strength, and variable magnetic field sources in magnetic suspension applications. Composed of two nested axial-flux Halbach cylinders, this device can control the attraction force on a ferromagnetic plate by rotating one of the rings relative to the other. These characteristics were seen in both computer simulations and the physical prototype. Through modeling, we found that the CAHA outperforms alternative controllable magnetic field sources, requiring less power for low frequency tasks than electromagnets and having higher forces and force ranges at large gap distances than switchable permanent magnets. And compared to an adjustable planar Halbach array in which many magnetized rods must spin [21], the CAHA is a simpler device where only one ring must move.

In low-frequency magnetic suspension tasks, the major power reduction of the CAHA with respect to electromagnets would greatly reduce cooling requirements and extend the life of battery-powered systems. This is because the load torque on the CAHA motor is primarily a function of the ring turning torque (T_r in Eq. 2) when $\ddot{\theta}_r$ is low, and the power required to produce T_r is low. The 5 Hz force profile case exemplifies this power reduction, where the CAHA only consumed between 7% (inner ring rotates) and 17% (outer ring rotates) of the average power of the best electromagnet (Fig. 3b). In high-frequency applications, electromagnets have the advantage over the CAHA, because high power is required to accelerate the ring's inertia when $\ddot{\theta}_r$ is high. As frequency (ω) increases, the power requirements of the CAHA increase quadratically because the $\ddot{\theta}_r$ term in Eq. 2 increases proportional to ω^2 for $\theta_r \approx sin(\omega t)$. One limitation of this comparison is that we only modeled a simple

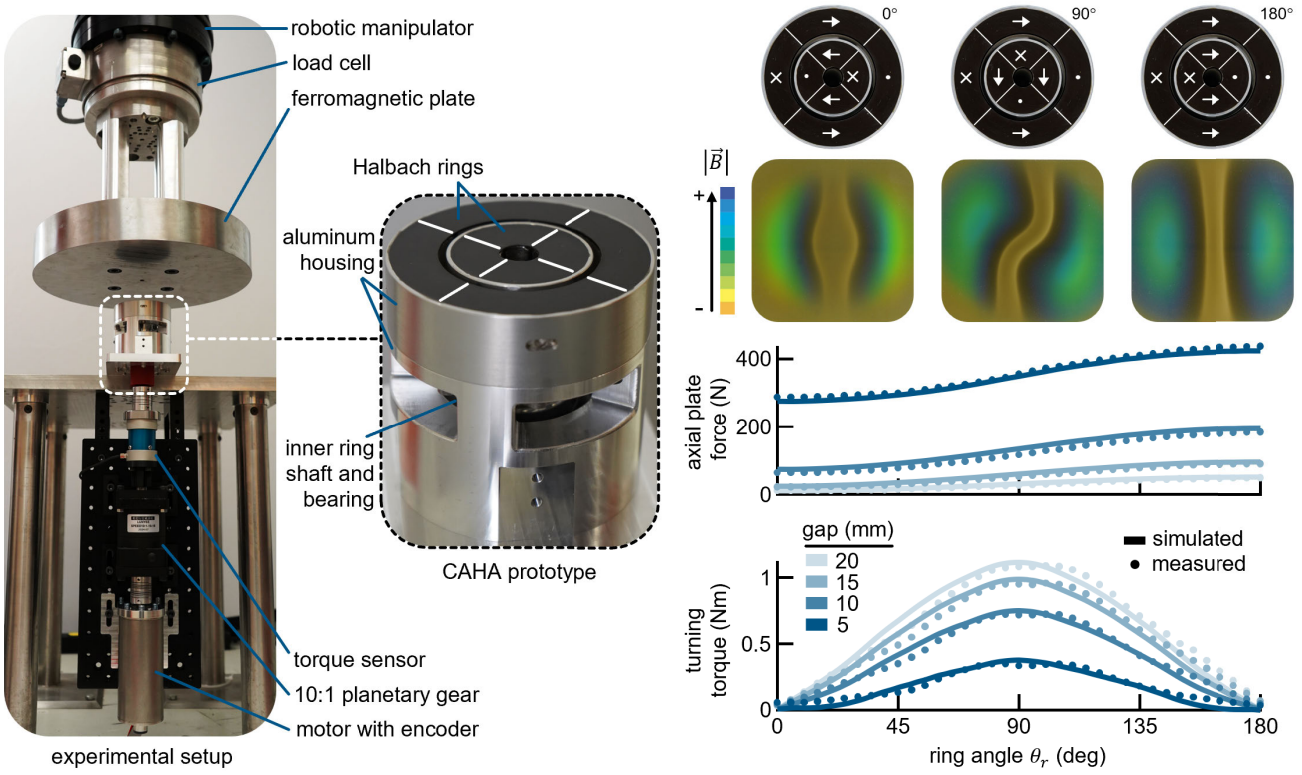

FIGURE 7. Empirical characterization of the CAHA prototype specified in Table 2. (a) The physical test stand consisted of the CAHA prototype mounted vertically on a table. The inner ring of the CAHA was turned by a motor through a 10:1 planetary gear. The CAHA angle was measured by the motor encoder and the turning torque was measured by an in-line torque sensor. A large ferromagnetic plate was attached to a robotic manipulator, such that the gap distance between the bottom of the plate and the top of the CAHA could be adjusted. The force on the plate was measured by a load cell on the manipulator's end effector. (b) Experimental CAHA characterization. At the top, magnetic viewing film placed 27.5 mm above the CAHA shows relative magnitudes of magnetic flux density for ring angles of 0°, 90°, and 180°. The two lower plots show the axial force exerted on the ferromagnetic plate and the torque required to turn the inner ring as a function of ring angle for four gap distances. JMAG simulation results of this test are plotted as solid lines while points show measured values.

ferritic-cored electromagnet. Although this represents the most common form of electromagnet, other electromagnet architectures can reduce power requirements in magnetic suspension tasks. These include replacing the ferromagnetic core with a permanent magnet [6] or using advanced materials [25]. Despite these improvements, all electromagnets fundamentally rely on power to maintain any field other than their unpowered field; while a permanent magnet core or better materials could shift the average power requirements downward, there would still be a low-frequency region in which the CAHA is favorable. Another limitation of our electromagnet comparison is that for the full CAHA-based actuator (CAHA rings and motor), the mass of the CAHA actuator is similar to that of the electromagnet, but the electromagnet is smaller than the CAHA actuator. This is because the electromagnet was designed to be the same dimensions as the two CAHA rings by themselves not including the motor. Allowing for a larger electromagnet of the same size as the combined CAHA rings and motor thus could have decreased the power requirements of the electromagnet in 3, however this electromagnet would be much heavier than the CAHA actuator. In a similar argument to using different core materials, there would also still be a low-frequency region in which the CAHA-based actuator was favorable.

For large gap ($\geq$ 10 mm) applications, the higher forces produced by the CAHA compared to the SM are important for enabling high-force tasks or reducing the size of existing magnetic suspension systems. The greater force density of the CAHA in these regions also shows how the CAHA outperforms SMs for a given mass. At a 20 mm gap, the CAHA produced almost twice the maximum force of the best SM design (Fig. 4a) while being similar masses. For low gaps, however, the ability of the SM to achieve low minimum forces resulted in greater performance than the CAHA. This suggests that the benefit of using a CAHA over a SM for applications, such as climbing robots, depends on the expected gap distance regime. It is also important to recognize that at lower gap distances, the CAHA seems to lose the ability to turn "off" when the rings are anti-

aligned ($\theta_r = 0°$). At the lowest gap we tested (1 mm), this effect was so pronounced that the CAHA produced a higher force when the rings were anti-aligned. While out of the scope of this paper, we hope to investigate this phenomenon in subsequent work. Depending on the application, the reduced force range of the CAHA at lower gap distances may not be as important as the higher maximum forces it can produce. One example of this would be suspending a mass in free space, since the position of the mass can be controlled as long as its weight and acceleration forces are within the minimum and maximum CAHA force. In this case, the CAHA could be the better choice despite a smaller force range if the SM cannot provide the required force.

There are several CAHA parameters that can be tuned for different applications. Looking at the wavenumber, k, of the CAHA, we found that the $k = 1$ CAHA had higher maximum forces and force ranges at large gaps than arrays with $k = 2$ or $k = 3$ (Fig. 5b). Lower k also reduced the torque required to turn the arrays, which is advantageous for physical implementations by reducing actuator loads. For applications with gap distances below 10 mm, arrays with higher k should be used, because these can produce higher forces and maintain larger force ranges. The problem of higher turning torque for arrays with higher k is also mitigated for lower gaps because the turning torque decreases with gap distance. Sweeping the geometric parameters, we found that the best way to increase performance for the CAHA was to increase either the the height or the outer radius. Between these two, an interesting differentiator was that maximum force and force range face diminishing returns for taller heights but not for larger radii. This should be expected because material added to the bottom of the CAHA will be farther away from the material to be attracted. Regardless of the overall dimensions, the parameter that should be carefully chosen is the thickness ratio (T_o/T_i), for which an optimal value does exist. For our pseudo-infinite plate, we found that a ratio of 0.5625 maximized the force range. Notably, this came at the expense of a higher maximum turning torque. When designing a CAHA for different applications, multiple thickness ratios should be tested to find the best value, as we did when creating the baseline CAHA. Another finding from the parameter sweep was that changing the bore radius of the CAHA did not have much effect on performance. This is a convenient feature for incorporating the CAHA into an actuator since the bore radius can be sized to fit a driveshaft to rotate the inner ring.

During testing of our physical CAHA prototype, the overall agreement between JMAG simulations and measured forces/torques show that this mechanism does behave as expected in reality. One interesting observation found in the measured turning torque characterization (bottom of Fig. 7b), however, is the presence of a "dimple" in the torque curves near $\theta_r = 90°$. This is most pronounced at lower gap distances, and was not observed in the simulation results. We plan to investigate this discrepancy in future electromagnetic modeling of the CAHA.

We intend this work to serve as an introduction to the design of our CAHA mechanism, and a general exploration of the applications for which it may be well-suited. We also sought to provide intuition for how specific design parameters affect CAHA performance, while leaving deeper experimental investigations into this device for subsequent testing. The close agreement between our simulations and empirical results provides confidence that the simulation-based analyses in this manuscript will translate to physical CAHA devices. Future work will tackle the development of a compact actuator system for real-world suspension tasks, and will also explore how to best integrate and control the CAHA. While our modeled actuator used a brushless motor with no transmission, one area of interest is optimizing the choice of transmission and motor paired with the CAHA to fully tailor the actuator to the chosen application.

V. CONCLUSION

Our novel controllable axial-flux Halbach array shows great potential as a low-power, high strength, adjustable magnetic field source. This device is particularly well-suited for low-frequency, large-gap magnetic suspension applications with an up to 93% reduction in average power compared to an electromagnet for a 5 Hz task along with a 2.3x higher force density than a switchable magnet at a 10 mm gap distance. Future research will further investigate the use of these arrays in specific magnetic suspension applications.

ACKNOWLEDGMENT

The authors thank Michael Rose for editorial advice. Will Flanagan and Tyler R. Clites are inventors on a patent related to this work.

REFERENCES

[1] M. Tavakoli, C. Viegas, J. C. Romão, P. Neto, and A. T. de Almeida, "Switchable magnets for robotics applications," in *Proc. IEEE/RSJ Int. Conf. Intell. Robots Syst. (IROS)*, Sep. 2015, pp. 4325–4330.

[2] A. Peidró, M. Tavakoli, J. M. Marín, and Ó. Reinoso, "Design of compact switchable magnetic grippers for the HyReCRo structure-climbing robot," *Mechatronics*, vol. 59, pp. 199–212, May 2019.

[3] H. Zhu, Z. Lin, J. Yan, P. Ye, W. Zhang, S. Mao, and Y. Guan, "Compact lightweight magnetic gripper designed for biped climbing robots based on coaxial rotation of multiple magnets," *Robot. Auto. Syst.*, vol. 155, Sep. 2022, Art. no. 104164.

[4] N. Shirazee and A. Basak, "Electropermanent suspension system for acquiring large air-gaps to suspend loads," *IEEE Trans. Magn.*, vol. 31, no. 6, pp. 4193–4195, Dec. 1995.

[5] H.-S. Han and D.-S. Kim, *Magnetic Levitation*. Cham, Switzerland: Springer Netherlands, 2016.

[6] W. Flanagan, K. Becraft, H. Warren, A. I. Stavrakis, N. M. Bernthal, T. J. Hardin, and T. R. Clites, "Prosthetic limb attachment via electromagnetic attraction through a closed skin envelope," *IEEE Trans. Biomed. Eng.*, vol. 71, no. 5, pp. 1–12, May 2024.

[7] R. Bjørk, C. R. H. Bahl, A. Smith, and N. Pryds, "Comparison of adjustable permanent magnetic field sources," *J. Magn. Magn. Mater.*, vol. 322, no. 22, pp. 3664–3671, Nov. 2010.
[8] K. Halbach, "Permanent multipole magnets with adjustable strength," *IEEE Trans. Nucl. Sci.*, vol. NS-30, no. 4, pp. 3323–3325, Aug. 1983.
[9] J. Mallinson, "One-sided fluxes—A magnetic curiosity?" *IEEE Trans. Magn.*, vol. M-9, no. 4, pp. 678–682, Dec. 1973.
[10] P. Jin, Y. Yuan, Q. Xu, S. Fang, H. Lin, and S. L. Ho, "Analysis of axial-flux Halbach permanent-magnet machine," *IEEE Trans. Magn.*, vol. 51, no. 11, pp. 1–4, Nov. 2015.
[11] G.-H. Jang, M.-M. Koo, J.-M. Kim, and J.-Y. Choi, "Torque characteristic analysis and measurement of axial flux-type non-contact permanent magnet device with Halbach array based on 3D analytical method," *AIP Adv.*, vol. 7, no. 5, Feb. 2017, Art. no. 056647.
[12] H. A. Leupold, E. Potenziani II, and M. G. Abele, "Applications of yokeless flux confinement," *J. Appl. Phys.*, vol. 64, no. 10, pp. 5994–5996, Nov. 1988.
[13] R. Bjørk, C. R. H. Bahl, A. Smith, and N. Pryds, "Review and comparison of magnet designs for magnetic refrigeration," *Int. J. Refrig.*, vol. 33, no. 3, pp. 437–448, May 2010.
[14] P. V. Trevizoli, J. A. Lozano, G. F. Peixer, and J. R. Barbosa Jr., "Design of nested Halbach cylinder arrays for magnetic refrigeration applications," *J. Magn. Magn. Mater.*, vol. 395, pp. 109–122, Dec. 2015.
[15] P. Blümler and H. Soltner, "Practical concepts for design, construction and application of Halbach magnets in magnetic resonance," *Appl. Magn. Reson.*, vol. 54, nos. 11–12, pp. 1701–1739, Dec. 2023.
[16] T. R. N. Mhiochain, D. Weaire, S. M. McMurry, and J. M. D. Coey, "Analysis of torque in nested magnetic cylinders," *J. Appl. Phys.*, vol. 86, no. 11, pp. 6412–6424, Dec. 1999.
[17] P. J. Underwood and F. Kocijan, "Switchable permanent magnetic device," U.S. Patent 6 707 360 b2, Mar. 16, 2004.
[18] T. Mizuno, M. Takasaki, M. Hara, D. Yamaguchi, and Y. Ishino, "Zero-power control of flux-path control magnetic suspension system with flux-interrupting plates," in *Proc. 11th Int. Symp. Linear Drives Ind. Appl. (LDIA)*, Sep. 2017, pp. 1–6.
[19] A. Garcia and M. Mehrubeoglu, "Switchable magnets as a power-efficient alternative for electromagnets in a mobile robotic system," in *Proc. IEEE Green Technol. Conf. (GreenTech)*, Apr. 2020, pp. 212–216.
[20] J. H. Kang, H. Driscoll, M. Super, and D. E. Ingber, "Application of a Halbach magnetic array for long-range cell and particle separations in biological samples," *Appl. Phys. Lett.*, vol. 108, no. 21, May 2016, Art. no. 213702.
[21] J. E. Hilton and S. M. Mcmurry, "An adjustable linear Halbach array," *J. Magn. Magn. Mater.*, vol. 324, no. 13, pp. 2051–2056, Jul. 2012.
[22] *NdFeB N52M Material Properties*. Accessed: Jun. 11, 2024. [Online]. Available: https://www.arnoldmagnetics.com/wp-content/uploads/2017/11/N52M-151021.pdf
[23] R. Bjørk, A. Smith, and C. R. H. Bahl, "The efficiency and the demagnetization field of a general Halbach cylinder," *J. Magn. Magn. Mater.*, vol. 384, pp. 128–132, Jun. 2015.
[24] U. H. Lee, C.-W. Pan, and E. J. Rouse, "Empirical characterization of a high-performance exterior-rotor type brushless DC motor and drive," in *Proc. IEEE/RSJ Int. Conf. Intell. Robots Syst. (IROS)*, Nov. 2019, pp. 8018–8025.
[25] A. Krings, M. Cossale, A. Tenconi, J. Soulard, A. Cavagnino, and A. Boglietti, "Magnetic materials used in electrical machines: A comparison and selection guide for early machine design," *IEEE Ind. Appl. Mag.*, vol. 23, no. 6, pp. 21–28, Nov. 2017.

WILL FLANAGAN (Member, IEEE) received the B.S. degree in mechanical engineering with a minor in physiology from Georgia Institute of Technology, Atlanta, GA, USA, in 2020. He is currently pursuing the Ph.D. degree with the Department of Mechanical and Aerospace Engineering, University of California at Los Angeles, Los Angeles, CA, USA.

HE KAI LIM received the B.S. degree in mechanical engineering from the University of California at Los Angeles (UCLA), Los Angeles, CA, USA, in 2023, where he is currently pursuing the Ph.D. degree with the Department of Mechanical and Aerospace Engineering. His research interests include the development and application of novel permanent magnet devices for biomechatronic applications, especially in addressing multidisciplinary clinical problems.

CAMERON R. TAYLOR received the B.S. degree in electrical engineering from Brigham Young University, Provo, UT, USA, in 2014, and the M.S. and Ph.D. degrees in media arts and sciences from Massachusetts Institute of Technology (MIT), Cambridge, MA, USA, in 2016 and 2020, respectively.

He held a Postdoctoral Scholar appointment with the Department of Mechanical and Aerospace Engineering, University of California at Los Angeles, Los Angeles, CA, USA, from 2023 to 2025. He is starting a position as an Assistant Professor of biomedical engineering with the University of North Carolina at Chapel Hill and NC State University, Chapel Hill, NC, USA, in 2025. His research interests include electromagnetics (particularly magnetoquasistatics), algorithm design, and bioinstrumentation.

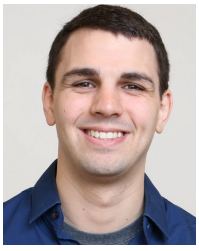

TYLER R. CLITES received the B.S. degree in engineering sciences from Harvard College, Cambridge, MA, USA, in 2014, and the dual Ph.D. degree in medical engineering and medical physics from the Health Sciences and Technology Program, Massachusetts Institute of Technology, Cambridge, and Harvard Medical School, Boston, MA, in 2018.

He is currently an Assistant Professor of mechanical and aerospace engineering, bioengineering, and orthopaedic surgery with the University of California at Los Angeles, Los Angeles, CA, USA. His research interests include the field of bionics, and more specifically anatomics, which he defines as coengineering of body and machine in pursuit of improved human function.